http://eprints.gla.ac.uk/201404/

1 **Influence of wet-dry cycles on vertical cutoff walls made of reactive**

2 **magnesia-slag-bentonite-soil mixtures**

3

4 Hao-Liang Wu

5 Jiangsu Key Laboratory of Urban Underground Engineering & Environmental Safety,

6 Institute of Geotechnical Engineering, Southeast University, Nanjing 210096, China.

7 Post-Doctoral Fellow, Department of Civil and Environmental Engineering, Hong

8 Kong University of Science and Technology, Hong Kong SAR, China. Email:

9 wuhaoliang@ust.hk

10

11 Fei Jin

12 Assistant Professor, School of Engineering, University of Glasgow, Glasgow G12 8QQ,

13 UK. Email: fei.jin@glasgow.ac.uk

14

15 Yan-Jun Du[*]

16 Professor, Jiangsu Key Laboratory of Urban Underground Engineering &

17 Environmental Safety, Institute of Geotechnical Engineering, Southeast University,

18 Nanjing 210096, China. Tel.: +862583793729; Fax: +862583795086,

19 [*]Corresponding author, Email: duyanjun@seu.edu.cn

20

23

Abstract

The strength and hydraulic conductivity of vertical cutoff walls consisting of reactive magnesia-activated ground granulated blast furnace slag (GGBS), bentonite and soil (MSB) have been investigated in previous studies. However, there has been little comprehensive study of the influence of wet-dry cycles on the mechanical and microstructural properties of MSB backfills. In this paper, the durability of MSB backfills when exposed to wet-dry cycles is investigated. The variations in mass change, dry density, pH value, pore size distribution and mineralogy are discussed. The results show that the mass change of Ordinary Portland Cement (OPC)-based and MSB backfills increases with respect to wet-dry cycles. The MSB backfills exhibit up to 8.2% higher mass change than OPC-based ones after ten wet-dry cycles. The dry density, pH value and unconfined compressive strength of MSB backfill decrease with the increasing number of wet-dry cycles. Increasing the GGBS-MgO content from 5% to 10% in MSB backfills results in 2.1 - 2.3 times higher strength, corresponding to a reduction of 2% - 12% in cumulative pore volume; while increasing the bentonite content slightly reduces the strength of MSB mixtures, corresponding to an increase of cumulative pore volume by 4.6% - 7.9%. The hydrotalcite-like phases and C-S-H are the primary hydration products in MSB backfills. Moreover, the continuous wet-dry cycles resulte in the precipitation of calcite ($CaCO_3$) and nesquehonite ($MgCO_3 \cdot 3H_2O$).

Keywords: Cutoff wall; reactive MgO-activated GGBS; durability; wet-dry cycles; carbonation

2

1. Introduction

The soil-cement-bentonite (SCB) cutoff wall has been widely used worldwide in remediation projects for contaminated sites (Ryan and Day 2002; Opdyke and Evans 2005; Ruffing and Evans 2014). Such walls have been mainly used to interrupt the pollution pathway and to isolate the contaminant source from a vulnerable receptor (Joshi et al. 2008; Soga and Joshi 2015; Du et al. 2015; Yang et al. 2018 and 2019). As compared to soil-bentonite (SB) and cement-bentonite (CB) cutoff walls, SCB walls possess adequate strength to carry foundation loads. They have the additional economic merit of the reuse of site-excavated soils (Ryan and Day 2002; Opdyke and Evans 2005). In CB and SCB walls, Ordinary Portland cement (OPC) is the primary cementitious material used, and is associated with intensive CO_2 emissions (0.95 t/t OPC) and consumption of raw materials (Benhela et al. 2013). In recent years, many industrial by-products such as ground granulated blast furnace slag (GGBS) and fly ash have become popular as partial substitutions for OPC in geotechnical applications (Jefferis 2012; Lam and Jefferis, 2017; Arulrajah et al. 2017a; Arulrajah et al. 2017b; Wu et al. 2019). For example, replacing OPC with GGBS in the cutoff wall backfill has been applied extensively in the UK (Jefferis 2012). It has significant environmental and economic benefits, marginally affects the q_u (sometimes with enhancement), slightly decreases pore water pH and notably decreases hydraulic conductivity in the long term (Wu et al. 2019).

Compared to OPC, using reactive MgO as the activator for GGBS has many potential technical benefits, in particular for soil remediation applications. The main

67 hydration products in reactive MgO-activated GGBS are calcium silicate hydrate (C-S-

68 H), hydrotalcite and brucite ($Mg(OH)_2$, if MgO is excessive) (Du et al. 2016; Jin et al.

69 2015; Jin and Al-Tabbaa 2014a; Wang et al. 2016; Yi et al. 2013). Due to the absence

70 of highly soluble portlandite with a high equilibrium pH value (~12.5) and the

71 formation of the above-mentioned products with excellent adsorptive capacities, MgO-

72 GGBS blends have shown superiority over OPC for contaminant immobilization in a

73 number of laboratory studies and field trials (Du et al. 2016; Jin et al. 2015; Jin et al.

74 2016; Jin and Al-Tabbaa, 2014a and b; Wang et al. 2016).

75   Recently, this novel cement has been applied to form an innovative cutoff wall

76 backfill material, together with bentonite and site sandy soil (MSB) (Wu et al. 2019).

77 The unconfined compressive strength (q_u) and hydraulic conductivity (k_w) of the

78 proposed backfill permeated with tap water are in the range of 230 - 520 kPa and

79 1.1×10^{-10} - 6.3×10^{-10} m/s at 90-day-curing, respectively, complying well with the

80 commonly adopted design limits ($q_u \geq 100$ kPa and $k_w \leq 1.0\times10^{-8}$ m/s) (ICE 1999; Ryan

81 and Day 2002;). More importantly, this backfill showed excellent durability under

82 exposure to sodium sulfate (Na_2SO_4) or lead-zinc (Pb-Zn) solutions (Wu et al. 2019).

83 Environmental and cost assessments demonstrated that this innovative MSB backfill

84 material reduced CO_2 emissions by 85% with ~15.3% - 16.9% lower cost when

85 compared with OPC-based SCB backfills.

86   In a scenario of cutoff wall installations, the groundwater levels at each side of the

87 barrier may fluctuate over time (Evans 1991; Ross and Beljin 1998). The potential

88 changes in the q_u and k_w of the cutoff wall exposed to cyclic wet-dry actions have been

89   recognized as a medium- to long-term performance concern (Malusis et al., 2011;

90   National Research Council, 2007; Soga and Joshi, 2015). For CB and SCB walls,

91   noticeable cracks were observed due to shrinkage in the drying phase (Soga and Joshi

92   2015), which would lead to the increase of k_w by 2 - 3 orders (Joshi et al., 2009).

93   Previous studies also illustrated that the q_u of MgO-GGBS stabilized kaolin clay

94   reduced dramatically with increasing wet-dry cycles (Du et al., 2016). Thus, it is

95   necessary to evaluate the durability of the innovative MSB backfill under wet-dry

96   cycles.

97   This paper aims to investigate the effect of wet-dry cycles on the durability of

98   innovative MSB backfill. A series of laboratory tests, including mass change, dry

99   density, pH value, unconfined compression tests, Mercury Intrusion Porosimetry (MIP)

100   and X-ray diffraction (XRD) are performed in order to reveal the effects of wet-dry

101   cycles on the properties of MSB backfills.

102   **2. Materials and specimen preparation**

103   2.1 Solid materials

104   The backfill materials were prepared using Nanjing local soil, powdered sodium

105   activated calcium-bentonite, MgO and GGBS. The Nanjing local soil is classified as a

106   clayey sand based on the Unified Soil Classification System (ASTM 2017). The

107   commercial powdered sodium activated calcium-bentonite was provided by the

108   MuFeng mineral processing plant in Zhenjiang, China. GGBS and MgO used in this

109   study were obtained from Nanjing and Jinan, China, respectively. The physicochemical

110   properties for the site soil and bentonite are shown in **Table 1**. The moisture and specific

gravity were measured according to ASTM D2216 (ASTM, 2010a) and ASTM D4318 (ASTM, 2010b), respectively. The pH was measured by ASTM D4972 (ASTM, 2018a) using a pH meter HORIBAD-54. The cation exchange capacity was measured as in ASTM D7503 (ASTM, 2010c). The specific surface area was measured by nitrogen adsorption using a Physisorption Analyzer ASAP2020 according to (Cerato and Lutenegger, 2002). The medium reactivity MgO (reactivity is 102 s, determined by the acetic acid test according to Shand (2006)) was selected due to its appropriate reactivity and cost (Wu et al., 2018a and b; Jin and Al-Tababa, 2014c). The chemical compositions of the soil, GGBS and MgO used for this study are shown in **Table 2**, as measured by X-ray fluorescence (XRF) (ARL™ SMS-2000).

Table 1. Physicochemical properties of the local sandy-clay and bentonite

Index	Values			
	clayey sand	bentonite	GGBS	MgO
Moisture, (%)	4.81	11.2	-	-
pH (liquid to solid ratio at 1)	7.32	8.6	10.96	10.53
Specific gravity, G_s	2.62	2.66	-	-
Plastic limit, w_P (%)	-	55	-	-
Liquid limit, w_L (%)	-	103	-	-
Grain size distribution (%)				
Clay (<0.002 mm) [a]	5.62	99	-	-
Silt (0.002-0.075 mm) [a]	14.18	1	-	-
Sand (0.075-2 mm) [b]	80.20	-	-	-
Specific surface area, SSA (m^2/g)	-	378.5	0.29	28.02
Exchangeable cation (cmol/kg)				
Ca^{2+}		22.74		
Mg^{2+}		1.41		
Na^+		53.39		
K^+		0.53		
Sum		78.07		

[a] Measured using a laser particle analyzer Mastersizer 2000 (Malvern Instruments Ltd., UK)
[b] Measured with standard #10 - #200 sieves

Table 2. Chemical compositions of the clayed sand, OPC, GGBS and MgO (by wt%) used in this study determined by XRF

| Oxides	Clayey sand	OPC	GGBS	MgO
CaO	0.41	49.75	34.00	0.23
Al_2O_3	35.76	10.87	17.90	0.28
MgO	0.06	2.26	6.02	92.95
K_2O	0.15	0.75	0.64	0.01
SiO_2	48.73	22.6	34.3	0.28
Fe_2O_3	6.13	3.50	1.02	-
SO_3	0.07	3.84	1.64	0.45
MnO	0.11	0.24	0.28	0.01
Loss of ignition (%)	8.58	6.19	4.20	5.79

2.2 Backfill mix design and specimen preparation

Table 3 shows the mix proportions of the studied backfills. The MgO to GGBS ratio was 1:9 to achieve good strength and the lowest hydraulic conductivity based on preliminary studies (Jin et al., 2015; Wu et al., 2018a; Wu et al., 2019). The binder (OPC or GGBS-MgO) dosages (by weight of dry soil) ranged from 2.5% to 12.5% based on a review of previous studies (**Fig. 1**) as reported in Wu et al. (2019), which included both field and lab test results of SCB cutoff walls. Furthermore, since natural high-quality Na-bentonite in China is scarce, in practice engineers usually prefer to choose a higher dosage (≥5%) of sodium activated calcium-bentonite. The raw solid materials, including the clayey sand, powdered sodium activated calcium-bentonite, OPC or MgO and GGBS were weighed and mixed in a 2-L Hobart stainless steel mixer at 30 rpm for 5 min. It should be noted that the backfill specimens were prepared by mixing the non-prehydrated bentonite with sandy soil-OPC or sandy soil-GGBS-MgO mixture. Then the predetermined amount of tap water (pH = 6.8; EC = 3.3 μS/cm) was added and mixed at 60 rpm for 10 min to achieve homogeneity with the same slump value (150 ± 5 mm) (Wu et al., 2019). In the OPC-based backfill, the content of the

146 GGBS used in this study was 80% replacement of OPC, which was reported to exhibit

147 the lowest k_w and highest q_u (Opdyke and Evans, 2005). The mixtures were poured into

148 cylindrical moulds with sizes of Φ50 × H100 mm and cured for 90 days under

149 standard curing conditions ($T = 20 \pm 2$ °C, RH = 95%).
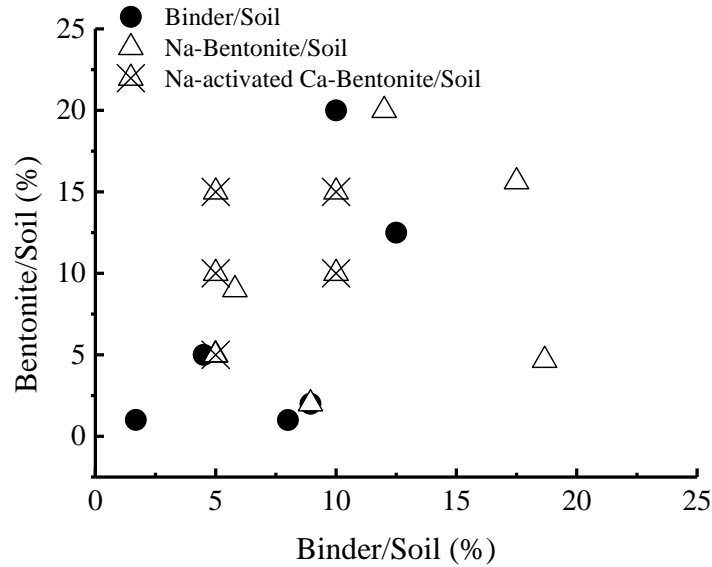
150

151 **Fig. 1 Summary of bentonite/soil and binder/soil ratios in SCB cutoff wall backfill mix**
152 **designs reported in previous studies (adapted from Wu et al., 2019)**

153

154 **Table 3. Mix design for the backfills used in this study (wt%)**

Category ID	Code	Clayey sand	Bentonite	OPC	GGBS	MgO
C	C5	100	-	5	-	-
CB	C5B5	100	5	5	-	-
	C10B10	100	10	10	-	-
CSB	CS5B5	100	5	1	4	-
	CS10B10	100	10	2	8	-
MSB	MS5B5	100	5	-	4.5	0.5
	MS5B10	100	10	-	4.5	0.5
	MS5B15	100	15	-	4.5	0.5
	MS10B10	100	10	-	9	1
	MS10B15	100	15	-	9	1

155

156 **3. Laboratory testing program**

157 The 90-day cured specimens were subjected to wet-dry cycles according to Kamon

158 et al. (1993). For each drying cycle, the specimens were stored in an oven (30 °C) for

159   48 h, followed by soaking in the distilled water with a temperature of 20 °C for 24 h.

160   The drying temperature was set as 30 °C to represent the typical average temperature

161   of hot seasons in the southeast regions of China and to minimize the effect of

162   accelerated slag hydration due to temperature rise (Du et al., 2016). The duration of

163   such a wet-dry cycle was three days and it was repeated for ten cycles.

164   After the ith wet or dry cycle, the mass change (MC) of the specimen is calculated

165   by Equation (1):

$$MC=(m_0-m_i)/m_0 \tag{1}$$

167   where m_0 = initial mass of the specimen measured prior to the wet-dry cycles, and

168   m_i = mass of the sample measured immediately after the ith drying cycle.

169   The densities of the specimens were measured in triplicate as in ASTM D7263

170   (2018b), and average values were reported. The specimens were subjected to UCT as

171   in ASTM D4219 (ASTM, 2008) with a strain rate of 1%/min. Fragments from the core

172   of the broken UCT specimens were air-dried, crushed and passed through a 2-mm sieve.

173   Ten grams of the sieved soil and 10 ml of distilled water (water to solid ratio = 1: 1)

174   were poured into a glass container to determine the pore water pH. The pH values of

175   the supernatant were measured by a HORIBA D-54 pH meter and the average value

176   was reported.

177   After the 10th wet-dry cycle, dry specimens were prepared to conduct MIP and

178   XRD tests. Briefly, ~1 cm^3 sample was collected from the specimen's core by a stainless

179   steel knife and frozen in liquid nitrogen. The frozen sample was dried in a vacuum

180   chamber at -80°C. The MIP tests were conducted according to ASTM D4404 (2010d)

181   using an Auto Pore IV 9510 mercury intrusion porosimeter to determine the pore size

182   distribution. Prior to XRD analysis, the dry specimens were ground and sieved to <

183   0.075 mm. The XRD spectra were obtained using a RigakuD/Max-2500 spectrometer

184   using a Cu-Kα source with a wavelength of 1.5405 Å. The instrument was operated at

185   40 kV and 20 mA. A step size of $2\theta = 0.02^{\circ}$ and a scanning speed of 5 s/step were used

186   over a range of 2θ from 10° to 50° in the step scan mode.

187

4. Results and Discussion

189   4.1 Mass change and visual inspection of physical integrity

190   **Fig. 2 (a)** and **(b)** present the variations in mass change with the wet-dry cycles

191   for the OPC-based and MSB backfills. It can be seen that the mass changes of the two

192   types of backfill increase with respect to the wet-dry cycles. Increasing the binder

193   content (GGBS-MgO) in the MSB backfills reduces mass change (by ~ 9.0 - 11%) (i.e.,

194   comparing MS10B10 and MS10B15 with MS5B10 and MS5B15, respectively). **Fig. 2**

195   **(b)** also indicates that increasing the bentonite content from 5% to 15% leads to a higher

196   mass change for the MSB backfills. This is attributed to the fact that higher bentonite

197   content (i.e., MS5B15) is more sensitive to the loss of water as compared to MS5B5

198   and MS5B10, which would develop matrix suction and increase the shrinkage in the

199   backfills in the drying stages (Nahlawi and Kodikara, 2006; Rowe et al., 2011; Tang et

200   al., 2011). However, the binder and bentonite contents show no significant impact on

201   the OPC-based backfills as shown **Fig. 2 (a)**. After the last wet-dry cycle, the mass

202   changes in MSB backfills reach approximately 12 - 19%, and are slightly higher than

203 those for the OPC-based backfills. Meanwhile, the mass change is much higher in MSB

204 than OPC at the wetting stage; the difference is much smaller at the drying stage. This

205 may imply that the water absorption potential of the bentonite in MSB mixtures is better

206 preserved than that in OPC-based mixtures. It was also found that spalling and macro-

207 cracks started to develop at the 4th - 6th cycles and were exacerbated with each wet-dry

208 cycle, as shown in **Fig. 3**.
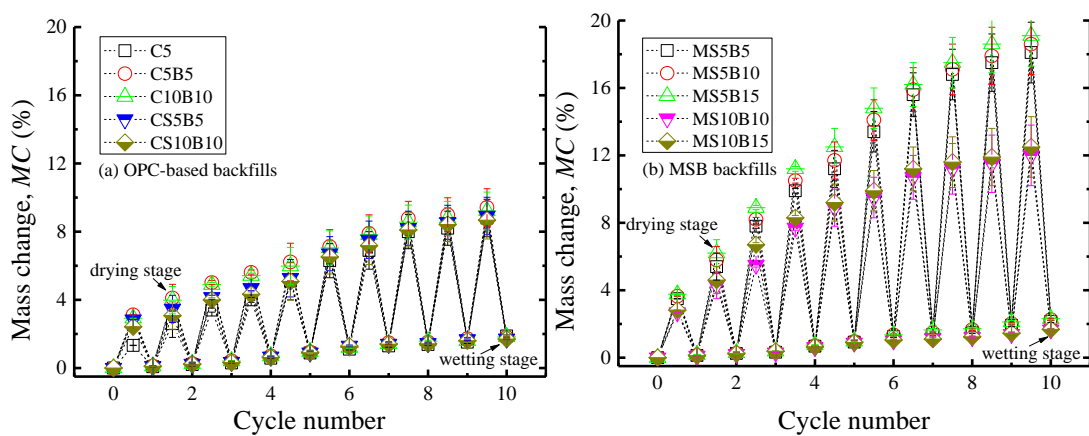
209

210 **Fig. 2 Variations in mass change with wet-dry cycles for (a) OPC-based and (b) MSB**
211 **backfills**

212
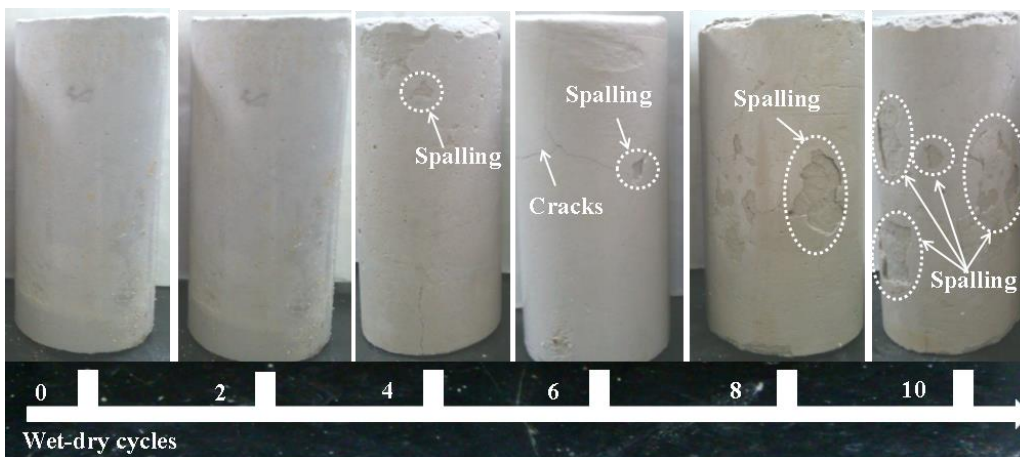
213

214 **Fig. 3 Photos showing the physical integrity of MSB backfills during wet-dry cycling**

215 4.2 Dry density

216 **Fig. 4** shows the variations of average values and standard deviations (STD) of

217 dry densities with wet-dry cycles for OPC-based and MSB backfills. The dry densities

218 of OPC-based and MSB backfills are 1.34 - 1.39 g/cm^3 and 1.31 - 1.35 g/cm^3 after the

219 10th wet-dry cycles, respectively. For all backfills, the dry density decreases slightly

220 with the wet-dry cycles, which is consistent with the mass change evolution as shown

221 in **Fig. 2**. For the identical binder and bentonite content, it is found that the dry density

222 of MSB backfills (i.e., M5B5) is higher than that of OPC-based backfills (i.e., C5B5

223 and CS5B5) after being exposed to ten wet-dry cycles. This may be attributed to the

224 fact that the C-S-H gels formed in GGBS-MgO have a lower Ca/Si ratio compared to

225 those formed in OPC, leading to higher shrinkage during the drying process (Du et al.,

226 2016; Jin et al., 2014b). At the same bentonite content in MSB backfills, the increase

227 of GGBS-MgO content has only a slight impact on the dry density (i.e., comparing

228 MS10B10 and MS10B15 with MS5B10 and MS5B15, respectively) whereas the dry

229 density significantly decreases as the bentonite content increases from 5% to 15% at

230 the identical GGBS-MgO content (i.e., comparing MS5B5 with MS5B10 and MS5B15)
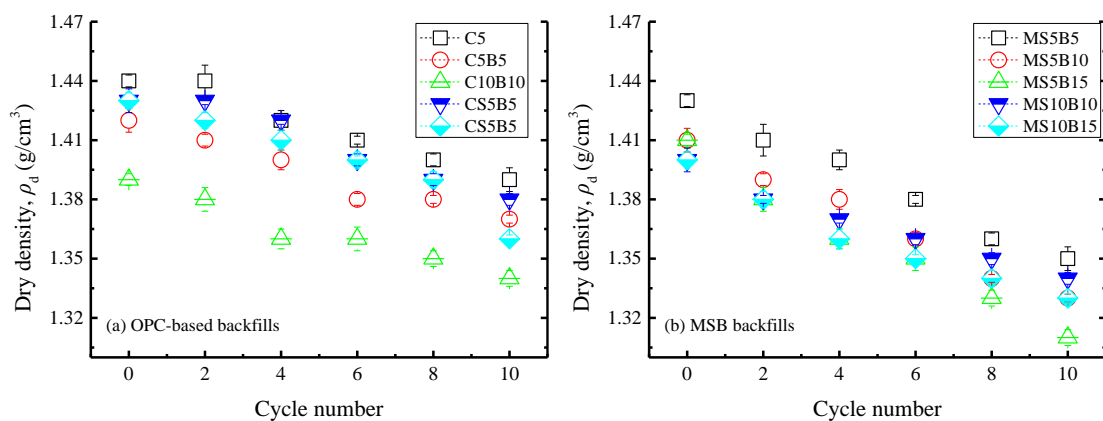
231 after ten wet-dry cycles.

232

233 **Fig 4. Dry density values for backfills after wet-dry cycles**

234 4.3 pH value

235 **Fig. 5** depicts the variations in the soil pH values with the wet-dry cycles for OPC-

based and MSB backfills. It can be observed that the pH for all backfills gradually

decreases with increasing wet-dry cycles. This is attributed to the leaching of alkaline

substances (i.e., Ca^{2+}) from the backfills when exposed to wetting. After ten wet-dry

cycles, the pH of OPC-based and MSB backfills are 10.9 - 12.3 and 9.8 - 10.8,

respectively. At the same binder and bentonite contents, the pH values of MSB backfills

are much lower than those of OPC-based backfills either before or after the wet-dry

cycles. For instance, the pH values for 5% GGBS-MgO in MSB backfills (i.e., MS5B5

and CS5B5) are approximately 0.5 - 1.2 lower than those for 5% OPC-based backfills

(i.e., C5B5 and CS5B5) after ten wet-dry cycles. Increasing the bentonite content in

MSB backfills reduces the pH values by 0.4 and 0.2 unit at 5% and 10% binder contents

(i.e., comparing MS5B10 and MS10B10 with MS5B15 and MS10B15, respectively)

after ten wet-dry cycles. Increasing the GGBS-MgO content results in higher pH, while

increasing the bentonite content decreases the pH value in the MSB mixtures.
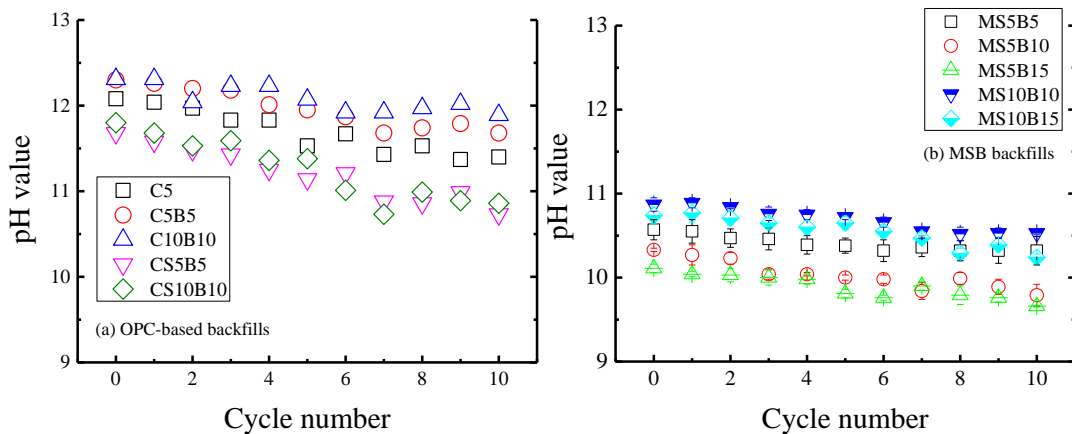
Fig. 5 Variations in pH with wet-dry cycles for (a) OPC-based and (b) MSB backfills

4.4 Unconfined compressive strength

Fig. 6 shows the evolution of q_u for the OPC-based and MSB specimens. It is found

that q_u values of the two types of backfill decrease with increasing wet-dry cycles. After

ten wet-dry cycles, the q_u values of the OPC-based and MSB backfills are 400 – 540

kPa and 180 – 420 kPa, respectively. The decreased q_u is attributed to the gradually

dissolved Ca^{2+} from the OPC-based and MSB matrices exposed to wetting conditions

(Du et al., 2016; Shen et al., 2008). As the pH decreases to below 10.8 (**Fig. 5**), the

partial destruction of C-S-H gels in the MSB backfill matrix also leads to lower q_u

when compared to OPC-based backfills (**Fig. 6**). For the MSB backfills, the q_u of 10%

GGBS-MgO in MSB backfills (i.e., MS10B10 and MS10B15) is 2.1 - 2.3 times higher

than that of 5% GGBS-MgO (i.e., MS5B10 and MS5B15). It is also observed that

increasing the bentonite content at the same binder content slightly reduces the strength

of MSB mixtures, and that is consistent with the higher mass change and lower dry

density shown in **Fig. 2** and **Fig. 4**.

The strength loss (*SL*) and cumulative strength loss (*CSL*) is computed by

Equations (2) and (3).

$$SL_i=(q_{u0}-q_{ui})/q_{u0} \tag{2}$$

$$CSL=\sum_{i=0}^{10} SL_i \tag{3}$$

where q_{u0} = initial unconfined compressive strength of the specimen measured prior to

the wet-dry cycles, and q_{ui} = mass unconfined compressive strength of the sample

measured immediately after the ith wet-dry cycle.

It can be observed that the *CSL* for 5% GGBS-MgO backfills (i.e., MS5B10 and

MS5B15) is 35% - 47% higher than that of 10% GGBS-MgO (i.e., MS10B10 and

MS10B15) as shown in **Fig. 7**. Furthermore, *CSL* decreases by 2.7% and 6.4% for 5%

and 10% GGBS-MgO in MSB backfills, respectively, as the bentonite increases from

277 10% to 15%. Thus, the impact of wet-dry cycles on MSB backfills is greater than on

278 OPC-based backfills. This phenomenon might be attributed to: (i) a lower Ca/Si ratio

279 of C-S-H in MSB backfills as compared to that formed in the OPC-based backfills,

280 which is more prone to shrinkage under the drying process, resulting in micro-cracking

281 of the matrix (Jin et al., 2014b) and (ii) a larger amount of uncombined water remaining

282 in the MSB backfills due to the better preserved bentonite swelling/shrinkage behavior

283 (Wu et al., 2019), which is prone to evaporation and leads to substantial shrinkage

284 cracking upon drying, resulting in greater strength loss.
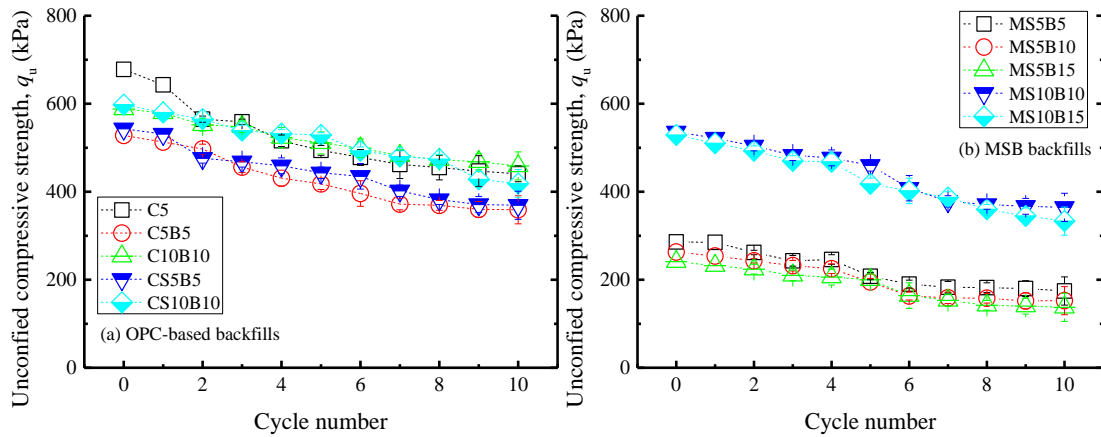
Fig. 6 Effective of wet-dry cycles on q_u for (a) OPC-based and (b) MSB backfills
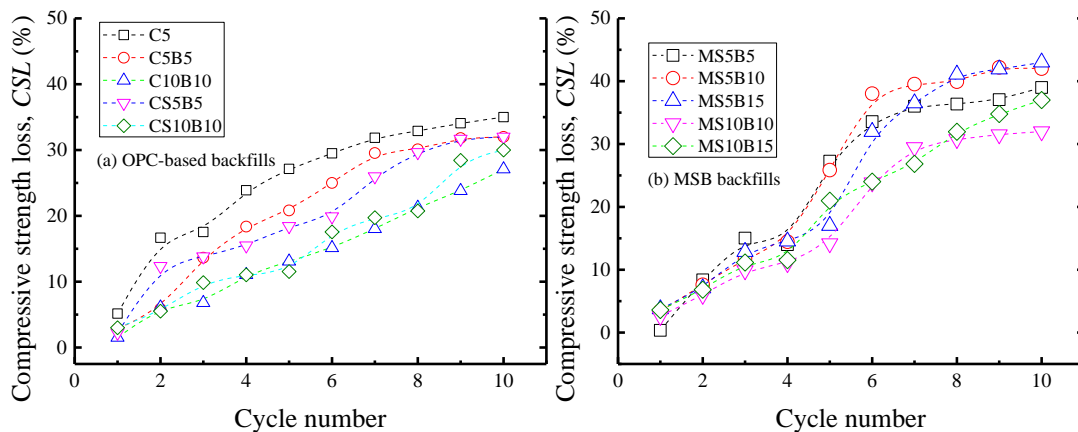
Fig. 7 Effect of wet-dry cycles on cummulative strength loss for (a) OPC-based and (b) MSB backfills

4.5 Pore size distribution

    To investigate the evolution in pore profiles of MSB backfills with respect to wet-

15

292   dry cycles, MIP tests are conducted. **Fig. 8 (a)** shows the cumulative pore volumes of

293   the MSB backfills after ten wet-dry cycles. At the same bentonite content, the

294   cumulative pore volumes of MS5B10 and MS5B15 are found to decrease by 12% and

295   2% as compared with MS10B10 and MS10B15. At 5% GGBS-MgO content, increasing

296   the bentonite content from 5% to 10% and 15% increases the cumulative pore volume

297   by 4.6% and 7.9%, respectively. The results for the pore profiles are consistent with the

298   observed trends for q_u and mass change as shown in **Fig. 6 (b) and Fig 2 (b).**

299   **Fig. 8 (b)** shows the volumes of the pores in different size ranges: <0.01 μm (intra-

300   aggregate), 0.01 – 10 μm (inter-aggregate) and >10 μm(air pores) respectively. This

301   classification of pore sizes is suggested by Horpibulsuk et al., (2010) and Xia et al.,

302   (2018 and 2019) for the OPC stabilized silty clay. Regardless of the binder content, the

303   proportions of air pores and inter-aggregate pores decrease but intra-aggregate pores

304   increase as the bentonite content increases from 5% to 15%. At the same bentonite

305   content, increasing the binder content decreases the proportions of pores in each

306   category (i.e., comparing MS5B10 and MS10B10 with MS5B15 and MS10B15). As

307   reported in previous studies (Collins and Sanjayan, 2000; Du et al., 2014 and 2016), a

308   larger volume of inter-aggregate pores can lead to higher drying-initiated capillary

309   tension forces and greater shrinkage potential in the matrix. Thus, the MS10B10

310   mixture shows the highest q_u and least mass change among all the MSB backfills as

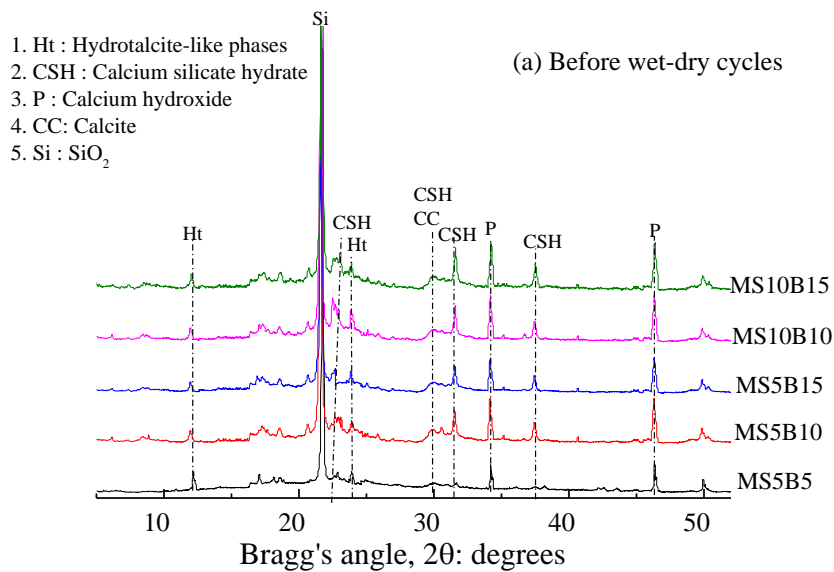311   shown in **Fig. 6** and **Fig. 2**.
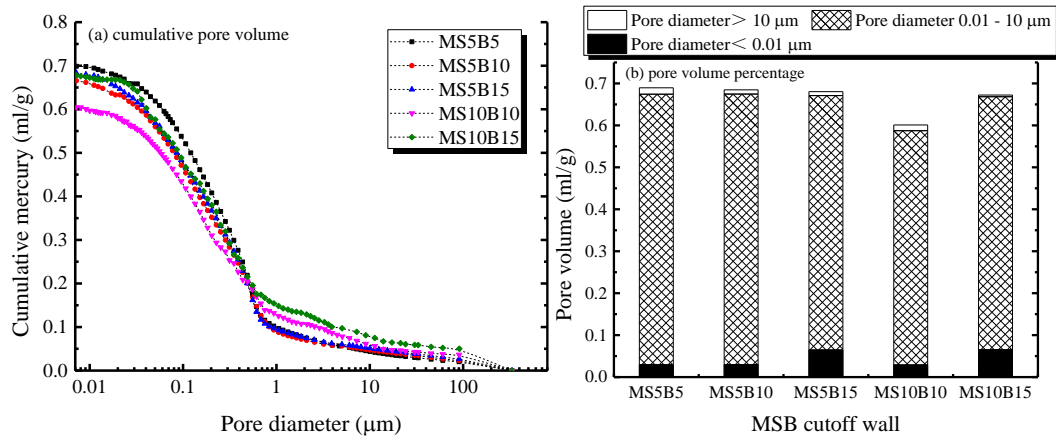
Fig. 8 The (a) cumulative pore volume and (b) pore volume percentage of MSB backfills after 90 days standard curing and subjected to ten wet-dry cycles

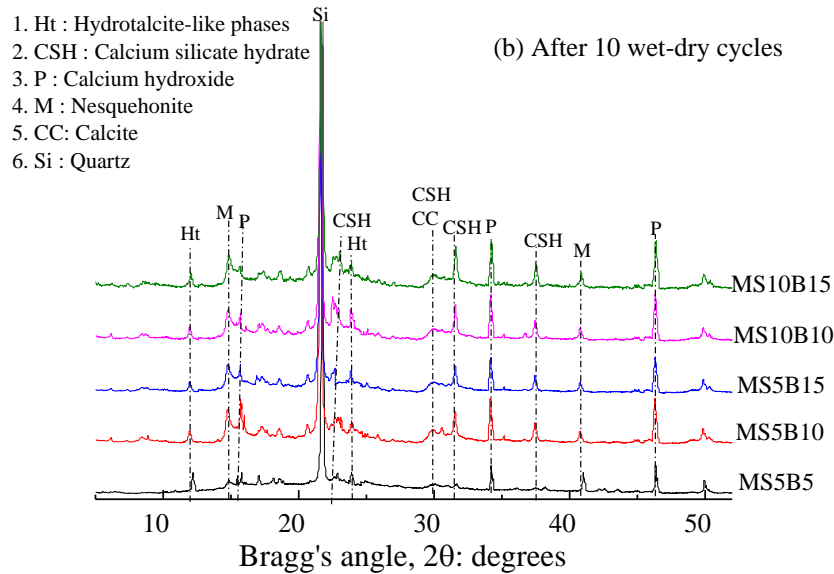4.6 X-ray diffraction

XRD tests were conducted on the MSB specimens before and after ten wet-dry cycles to investigate the evlolution of the phase assemblage in the mixtures as presented in **Fig. 9 (a)** and **(b)**. The characteristic peaks of hydrotalcite $(Mg_6Al_2(OH)_{16}CO_3 \cdot 4H_2O)$-like phases (Ht) were found at $2\theta \approx 12.5°$ and $24.0°$, agreeing well with previous findings (Jin et al., 2014a). In addition, two broad peaks ascribed to C-S-H were detected at $2\theta \approx 23.0°$, $30.0°$, $31.6°$ and $37.5°$, and were the result of the reaction between released silicate species and Ca from GGBS (Wu et al., 2019; Jin et al., 2014a and b). The C-S-H gels and hydrotalcite can improve the strength and hydraulic performance in MSB cutoff wall applications. Further, hydrotalcite has contaminants (e.g., lead and zinc) with a high capacity for adsorbtion and which therefore can enhance the chemical compatibility of the backfills exposed to contaminated underground conditions. The higher intensity of Ht and C-S-H are observed in 10% GGBS-MgO (i.e., MS10B10 and MS10B15) as compared with 5% GGBS-MgO (i.e., MS5B5, MS5B10 and MS10B15), and result in higher q_u (**Fig. 6**)

17

and lower mass change (**Fig. 2**). The characteristic peak of quartz (SiO_2) has been

detected at $2\theta \approx 21.6°$ in the local clayey sand. The characteristic peaks of calcium

hydroxide ($Ca(OH)_2$) have been detected at $2\theta \approx 19.0°$, $34.5°$ and $46.5°$, from the

leaching of Ca^{2+} from GGBS and C-S-H. The leaching of Ca^{2+} will lead to the decrease

of pH value as illustrated in **Fig. 5**. Nesquehonite ($MgCO_3.3H_2O$) is found in the

backfills after ten wet-dry cycles, as the peaks at $2\theta \approx 14.2°$ and $41.0°$) agree with those

reported by Wu et al., (2018b) and Ruan et al. (2019) It is formed by the dissolved Mg^{2+}

from the MSB backfills and dissolved CO_2 from the atmosphere. Similarly the leached

Ca^{2+} from the GGBS and C-S-H may react with dissolved atmospheric CO_2 to form

calcite. Nevertheless, the strongest calcite peak ($2\theta \approx 30.0°$) overlaps with that of C-S-

H, which prevents its identification via XRD in this study.

1. Ht : Hydrotalcite-like phases
2. CSH : Calcium silicate hydrate
3. P : Calcium hydroxide
4. CC: Calcite
5. Si : SiO_2

(a) Before wet-dry cycles

Fig. 9 X-ray diffractograms of the 90-day cured MSB backfills before (a) and after (b) wet-dry cycles: Ht: Hydrotalcite-like phases, CSH: Calcium silicate hydrate, P: Calcium hydroxide, M: Nesquehonite, CC: Calcite, Si: Quartz

5. Limitations of current study

This study reveals that the MSB mixture is more sensitive to a fluctuating groundwater condition than OPC-based backfills. This might be attributed to the hydration products (C-S-H with lower a Ca/Si ratio) and microstructure (refined pores) formed in alkali-activated GGBS paste as compared to OPC-based backfills (Du et al., 2015). Nevertheless, the unconfined compressive strength values of MSB mixtures are still above the commonly adopted design limits ($q_u \geq 100$ kPa) after ten wet-dry cycles. The much lower pH values of pore water in MSB mixtures have much weaker impact on the chemical stability of montmorillonite in bentonite as compared to OPC-based backfills (Wu et al., 2019). In addition, the use of a large amount of industrial waste gives the MSB mixture better sustainability than the OPC-based backfills.

Admittedly, for a full understanding of the long-term durability of the MSB backfills after wet-dry cycles, the wet-dry aging could be correlated with real time for a quantitative simulation (Shen et al., 2018 and 2019). Further investigations are

19

6. Conclusions

A comprehensive laboratory testing program was conducted to reveal the effects of wet-dry cycles on the properties of MSB backfills and the following conclusions can be drawn:

(1) The mass change of OPC-based and MSB backfills increased with respect to the wet-dry cycles. The MSB backfills exhibited 1.1% - 2.1% higher mass change than OPC-based ones after ten wet-dry cycles. Increasing the GGBS-MgO content reduced 9.0 - 11% mass change but increasing the bentonite content increased mass change in MSB backfills. The threshold cycle numbers for spalling and macro-cracks occurring in MSB backfills were found to be in the 4th- 6th cycles.

(2) The dry density and pH of OPC-based and MSB backfills gradually decreased with increasing wet-dry cycles. For the identical binder (OPC and GGBS-MgO) and bentonite contents, the mass change of MSB backfills was higher than in OPC-based backfills, while the pH was much lower.

(3) The unconfined compressive strength of OPC-based and MSB backfills decreased with increasing wet-dry cycles. The strength values of the MSB backfills with 10% GGBS-MgO were 2.1 - 2.3 times higher than those with 5% GGBS-MgO, while increasing the bentonite content slightly reduced the strength. The cumulative strength loss of MSB backfills was more notable than that for OPC-based backfills.

382   (4) Increasing the GGBS-MgO content from 5% to 10% reduces by 2% - 12% the

383 cumulative pore volume, while increasing the bentonite content from 5% to 15%

384 increases the cumulative pore volume by 4.6% - 7.9%.

385   (5) The hydrotalcite-like phases and C-S-H were found to be the primary hydration

386 products in the MSB backfills both before and after the wet-dry cycles. The wet-dry

387 cycles accelerated the leaching of earth alkali ions, which react with the dissolved CO_2

388 from the atmosphere to form calcite ($CaCO_3$) and nesquehonite ($MgCO_3 \cdot 3H_2O$) in

389 MSB mixtures.

390

396

References

Arulrajah, A., Kua, T. A., Horpibulsuk, S., et al., 2017. Recycled glass as a supplementary filler material in spent coffee grounds geopolymers. *Construction and Building Materials*, 151, 18-27. https://doi.org/10.1016/j.conbuildmat.2017.06.050

Arulrajah, A., Kua, TA., Suksiripattanapong, C., Horpibulsuk, S., et al., 2017. Compressive strength and microstructural properties of spent coffee grounds-bagasse ash based geopolymers with slag supplements. *Journal of Cleaner Production*, 162, 1491-1501. https://doi.org/10.1016/j.jclepro.2017.06.171

ASTM. 2008. Standard test method for unconfined compressive strength index of chemical-grouted soils. ASTM D4219. West Conshohocken, USA.

ASTM. 2010a. Standard Test Methods for Laboratory Determination of Water (Moisture) Content of Soil and Rock by Mass. ASTM D2216. West Conshohocken, USA.

ASTM. 2010b. Standard Test Methods for Liquid Limit, Plastic Limit, and Plasticity Index of Soils. ASTM D4318, West Conshohocken, USA.

ASTM. 2010c. Standard Test Method for Measuring the Exchange Complex and Cation Exchange Capacity of Inorganic Fine-Grained Soils. ASTM D7503. West Conshohocken, USA.

ASTM, 2010d. Standard test method for determination of pore volume and porevolume distribution of soil and rock by mercury intrusion porosimetry. ASTM D4404.

West Conshohocken, USA.

ASTM. 2014. Standard Test Methods for Specific Gravity of Soil Solids by Water Pycnometer. ASTM D4813. West Conshohocken, USA.

ASTM. 2017. Standard practice for classification of soils for engineering purposes (Unified Soil Classification System). ASTM D2487. West Conshohocken, USA.

ASTM. 2018a. Standard Test Method for pH of Soils. ASTM D4972. West Conshohocken, USA.

ASTM. 2018b. Standard test methods for laboratory determination of density (unit weight) of soil specimens. ASTM D7263. West Conshohocken, USA.

Benhelal, E., Zahedi, G., Shamsaei, E., and Bahadori, A. 2013. Global strategies and potentials to curb CO_2 emissions in cement industry. *Journal of Cleaner Production*, 51, 142-161. http://dx.doi.org/10.1016/j.jclepro.2012.10.049

Cerato, A. B., and Lutenegger, A. J. 2002. Determination of surface area of fine-grained soils by the ethylene glycol monoethyl ether (EGME) method. *Geotechnical Testing Journal*, 25(3), 315-321.

Collins, F., and Sanjayan, J. G. 2000. Effect of pore size distribution on drying shrinking of alkali-activated slag concrete. *Cement and Concrete Research*, 30, 1401–1406. https://doi.org/10.1016/s0008-8846(00)00327-6

Du, Y. J., Jiang, N. J., Liu, S. Y., et al., 2014. Engineering properties and microstructural characteristics of cement-stabilized zinc-contaminated kaolin. *Canadian Geotechnical Journal*, 51(3), 289-302.

441 https://doi.org/10.1139/cgj-2013-0177

442 Du, Y. J., Fan, R. D., Liu, S. Y., et al., 2015. Workability, compressibility and hydraulic

443   conductivity of zeolite-amended clayey soil/calcium-bentonite backfills for slurry-

444   trench cutoff walls. *Engineering Geology*, 195, 258-268.

445   https://doi.org/10.1016/j.enggeo.2015.06.020

446 Du, Y. J., Bo, Y. L., Jin, F., et al., 2016. Durability of reactive magnesia-activated slag-

447   stabilized low plasticity clay subjected to drying–wetting cycle. *European Journal*

448   *of Environmental and Civil Engineering*, 20(2), 215-230.

449   https://doi.org/10.1080/19648189.2015.1030088

450 Evans, J. C. 1991. Geotechnics of hazardous waste control systems. Foundation

451   engineering handbook, 2nd Ed., H. Y. Fang. ed., Van Nostrand Reinhold Company,

452   New York, N.Y. https://doi.org/10.1007/978-1-4757-5271-7_20

453 Horpibulsuk, S., Rachan, R., Chinkulkijniwat, A., et al., 2010. Analysis of strength

454   development in cement-stabilized silty clay from microstructural considerations.

455   *Construction and Building Materials*, 24(10), 2011-2021.

456   https://doi: 10.1016/j.conbuildmat.2010.03.011

457 ICE (Institution of Civil Engineers). 1999. Specification for the construction of slurry

458   trench cut-off walls as barriers to pollution migration. Thomas Telford, London.

459   https://doi.org/10.1680/sftcostcw.26254

460 Jefferis, S. 2012. Cement-bentonite slurry systems. Grouting and deep mixing, L. F.

461   Johnsen, D. A. Bruce, and M. J. Byle, eds., 1-24. Reston, VA, ASCE.

462   https://doi.org/10.1061/9780784412350.0001

463 Jin, F., and Al-Tabbaa, A. 2014a. Characterisation of different commercial reactive

464 magnesia. *Advances in Cement Research*, 26(2), 101-113.

465 https://doi.org/10.1680/adcr.13.00004

466 Jin, F., Gu, K., and Al-Tabbaa, A. 2014b. Strength and drying shrinkage of reactive

467 MgO modified alkali-activated slag paste. *Construction and Building Materials*,

468 51, 395–404.

469 https://doi.org/10.1016/j.conbuildmat.2013.10.081

470 Jin, F., and Al-Tabbaa, A. 2014c. Evaluation of novel reactive MgO activated slag

471 binder for the immobilization of lead and zinc. *Chemosphere*, 117: 285-294.

472 https://doi.org/10.1016/j.chemosphere.2014.07.027

473 Jin, F., Gu, K. and Al-Tabbaa, A. 2015. Strength and hydration properties of reactive

474 MgO-activated ground granulated blastfurnace slag paste. *Cement and Concrete*

475 *Composites*, 57, 8-16.

476 https://doi.org/10.1016/j.cemconcomp.2014.10.007

477 Joshi, K., Soga, K., Ng, M. Y. A., et al., 2008. Durability Study of Eleven Years Old

478 Cement-Bentonite Cut-Off Wall Material. *GeoCongress 2008: Geotechnics of*

479 *Waste Management and Remediation*, 620-627. New Orleans, LA, ASCE.

480 https://doi.org/10.1061/40970(309)78

481 Joshi, K., Kechavarzi, C., Sutherland, K., et al., 2009. Laboratory and in situ tests for

482 long-term hydraulic conductivity of a cement-bentonite cutoff wall. *Journal of*

483 *Geotechnical and Geoenvironmental Engineering*, 136(4), 562-572.

484 https://doi:10.1061/(asce)gt.1943-5606.0000248

485 Kamon, M., Nontananandh, S., and Katsumi, T. 1993. Utilization of stainless-steel slag

486 by cement hardening. *Soils and Foundations*, 118–129.

487 https://doi.org/10.3208/sandf1972.33.3_118

488 Kitazume, M., and Terashi, M. 2002. The deep mixing method principle, design and

489 construction. Tokyo: Balkema.

490 Lam, C., and Jefferis, S. A.. 2017. Polymer Support Fluids in Civil Engineering, ICE

491 Publishing, One Great George Street, Thomas Telford Limited, London.

492 https://doi.org/10.1680/psfce.57869

493 Liu, L., A. Zhou, Y. Deng, Y. Cui, Z. Yu, and C. Yu. 2019. Strength performance of

494 cement/slag-based stabilized soft clays. *Construction and Building Materials*, 211,

495 909-918.

496 https://doi.org/10.1016/j.conbuildmat.2019.03.25

497 Ma, L., Xu, D., S. Wang, S., et al., 2019. Expansion inhibition of steel slag in asphalt

498 mixture by a surface water isolation structure. *Road Materials and Pavement*

499 *Design,* 1-15.

500 https://doi.org/10.1080/14680629.2019.1601588

501 Malusis, M. A., Yeom, S., and Evans, J. C. 2011. Hydraulic conductivity of model soil–

502 bentonite backfills subjected to wet–dry cycling. *Canadian Geotechnical Journal*,

503 48(8), 1198-1211.

504 https://doi.org/10.1139/t11-028

505 Nahlawi, H., and Kodikara, J. K. 2006. Laboratory experiments on desiccation cracking

506 of thin soil layers. *Geotechnical and Geological Engineering*, 24(6), 1641-1664.

https://doi.org/10.1007/s10706-005-4894-4

National Research Council. 2007. Assessment of the performance of engineered waste containment facilities. The National Academies Press, Washington, D.C. https://doi.org/10.17226/11930

Opdyke, S. M., and Evans, J. C. 2005. Slag-cement-bentonite slurry walls. *Journal of Geotechnical and Geoenvironmental Engineering*, 131(6), 673-681.

Owaidat, L. M., Andromalos, K. B., Sisley, J. L., et al., 1999. Construction of a soil-cement-bentonite slurry wall for a levee strengthening program. In Proceedings of the 1999 Annual Conference of the Association of State Dam Safety Officials, St. Louis, Mo. 10-13.

Ross, R. R., and Beljin, M. S. 1998. Evaluation of containment systems using hydraulic head data. *Journal of Environmental Engineering*, 124(6), 575-578. https://doi.org/10.1061/(asce)0733-9372(1998)124:6(575)

Rowe, R. K., Bostwick, L. E., and Take, W. A. 2011. Effect of GCL properties on shrinkage when subjected to wet-dry cycles. *Journal of Geotechnical and Geoenvironmental Engineering*, 137(11), 1019-1027. https://doi.org/10.1061/(asce)gt.1943-5606.0000522

Ruan, S., Qiu, J., Weng, Y., et al., 2019. The use of microbial induced carbonate precipitation in healing cracks within reactive magnesia cement-based blends. *Cement and Concrete Research*, 115, 176-188. https://doi.org/10.1016/j.cemconres.2018.10.018

Ruffing, D. G., and Evans J. C. 2014. Case Study: Construction and In Situ Hydraulic

Conductivity Evaluation of a Deep Soil-Cement-Bentonite Cutoff Wall". *In Proc.,*

Geo-Congress 2014, 1863-1848. Atlanta, Georgia, ASCE.

https://doi.org/10.1061/9780784413272.180

Ryan, C. R., and Day S. R. 2002. Soil-cement-bentonite slurry walls. In Deep

foundations 2002: an international perspective on theory, design,construction, and

performance (Geotechnical Special Publication). 713-727.

https://doi.org/10.1061/40601(256)51

Shand, M. A. 2006. The chemistry and technology of magnesia, John Wiley & Sons.

Shen, S. L., Han, J., and Du, Y. J. 2008. Deep mixing induced property changes in

surrounding sensitive marine clays. *Journal of Geotechnical and*

Geoenvironmental Engineering, 134,845–854.

https://doi.org/10.1061/(asce)1090-0241(2008)134:6(845)

Shen, Z. T., Pan, S. Z., Hou, D., et al., 2019. Temporal effect of MgO reactivity on the

stabilization of lead contaminated soil. *Environment international*, 131, 104990.

https://doi.org/10.1016/j.envint.2019.104990

Shen, Z. T., Hou, D., Xu, W. D., Zhang, et al., 2018. Assessing long-term stability of

cadmium and lead in a soil washing residue amended with MgO-based binders

using quantitative accelerated ageing. *Science of the Total Environment*, 643,

1571-1578.

https://doi.org/10.1016/j.scitotenv.2018.06.321

Soga, K., and Joshi K. 2015. Cement bentonite cutoff walls for polluted sites. In Proc.,

Coupled Phenomena in Environmental Geotechnics, Taylor and Francis Group,

149-165.

https://doi.org/10.1201/b15004-15

Tang, C. S., Shi, B., Liu, C., et al., 2011. Experimental characterization of shrinkage and desiccation cracking in thin clay layer. *Applied Clay Science*, 52(1-2), 69-77.

https://doi.org/10.1016/j.clay.2011.01.032

Wang, F., Jin, F., Shen, Z., et al., 2016. Three-year performance of in-situ mass stabilised contaminated site soils using MgO-bearing binders. *Journal of Hazardous Materials*, 318, 302-307.

https://doi.org/10.1016/j.jhazmat.2016.07.018

Wu, H. L., Jin, F., Bo, Y. L., et al., 2018a. Leaching and microstructural properties of lead contaminated kaolin stabilized by GGBS-MgO in semi-dynamic leaching tests. *Construction and Building Materials*, 172, 626-634.

https://doi.org/10.1016/j.conbuildmat.2018.03.164

Wu, H. L., Zhang, D., Ellis, B. R., et al., 2018b. Development of reactive MgO-based Engineered Cementitious Composite (ECC) through accelerated carbonation curing. *Construction and Building Materials*, 191, 23-31.

https://doi.org/10.1016/j.conbuildmat.2018.09.196

Wu, H. L., Jin, F., Ni, J. et al., 2019. Engineering properties of vertical cutoff walls consisting of reactive magnesia-activated slag and bentonite: workability, strength and hydraulic conductivity. *Journal of Materials in Civil Engineering*. 31(11), 04019263.

https://doi.org/10.1061/(ASCE)MT.1943-5533.0002908

573   Xia, W. Y., Du, Y. J., Li, F. S., et al., 2019a. In-situ solidification/stabilization of heavy

574   metals contaminated site soil using a dry jet mixing method and new

575   hydroxyapatite based binder. *Journal of Hazardous Materials*, 369, 353-361.

576   https://doi.org/10.1016/j.jhazmat.2019.02.031

577   Xia, W. Y., Du, Y. J., Li, F. S., et al., 2019b. Field evaluation of a new hydroxyapatite

578   based binder for ex-situ solidification/stabilization of a heavy metal contaminated

579   site soil around a Pb-Zn smelter. *Construction and Building Materials*, 210, 278-

580   288.

581   https://doi.org/10.1016/j.conbuildmat.2019.03.195

582   Yang, Y. L., Reddy, K. R., Du, Y. J., et al., 2018. Short-term hydraulic conductivity

583   and consolidation properties of soil-bentonite backfills exposed to CCR-impacted

584   groundwater. *J Geotech Geoenviron Eng*, 144(6), 04018025.

585   https://doi.org/10.1061/(asce)gt.1943-5606.0001877

586   Yang, Y. L., Reddy, K. R., Du, Y. J., et al., 2019. Retention of Pb and Cr (VI) onto slurry

587   trench vertical cutoff wall backfill containing phosphate dispersant amended Ca-

588   bentonite. *Applied Clay Science*, 168, 355-365.

589   https://doi.org/ 10.1016/j.clay.2018.11.023

590   Yi, Y., Liska, M., Al-Tabbaa. 2013. A. Properties of two model soils stabilized with

591   different blends and contents of GGBS, MgO, lime, and PC. *Journal of Materials*

592   *in Civil Engineering*, 26, 267-274.

593   http://dx.doi.org/10.1061/(asce)mt.1943-5533.0000806